Acta Mechanica Solida Sinica, Vol. 27, No. 1, February, 2014 ISSN 0894-9166
Published by AMSS Press, Wuhan, China

ROTATIONAL RESISTANCE AND SHEAR-INDUCED ANISOTROPY IN GRANULAR MEDIA**

Jidong Zhao* **Ning Guo**

(*Department of Civil and Environmental Engineering, The Hong Kong University of Science and Technology, Clearwater Bay, Kowloon, Hong Kong, China*)

Received 12 February 2012, revision received 17 October 2013

ABSTRACT This paper presents a micromechanical study on the behavior of granular materials under confined shear using a three-dimensional Discrete Element Method (DEM). We consider rotational resistance among spherical particles in the DEM code as an approximate way to account for the effect of particle shape. Under undrained shear, it is found rotational resistance may help to increase the shear strength of a granular system and to enhance its resistance to liquefaction. The evolution of internal structure and anisotropy in granular systems with different initial conditions depict a clear bimodal character which distinguishes two contact subnetworks. In the presence of rotational resistance, a good correlation is found between an analytical stress-force-fabric relation and the DEM results, in which the normal force anisotropy plays a dominant role. The unique properties of critical state and liquefaction state in relation to granular anisotropy are also explored and discussed.

KEY WORDS granular media, anisotropy, discrete element method (DEM), rotational resistance, liquefaction, critical state

I. INTRODUCTION

Granular materials are important to our daily life. The handling of granular materials is common in civil, mining and chemical engineering, or agricultural, pharmaceutical and chemical industries. Sand, as a typical granular material, is commonly seen in nature as well as in engineering fields. Many important infrastructures pertaining to the quality and safety of our daily life, such as water dams, residential buildings, bridges, motorways, engineered slopes, embankments and foundations, are built in/on/with sand. The performance of sand under external loads may have a direct impact on the design, construction and operation of these structures[1]. Under shear, granular sand may exhibit extremely complicated behavior that draws wide attention in the community of soil mechanics as well as granular physics. Perplexing phenomena relevant to sand such as pressure and density dependency, anisotropy, dilatancy, combined isotropic and kinematic hardening, zero-dilation shear flow at critical state, non-coaxiality, liquefaction, as well as pattern formations and jamming transitions, have been subjects of intense recent studies[2–16]. The complicated behavior of granular media on the macroscopic level is known to be closely related to the complexity of their underlying microstructure as well as their effective macroscopic properties involving nontrivial detail of these microstructures[17]. Characteristics on the grain scale may contribute significantly to the overall complexity of granular materials[18–23].

* Corresponding author. E-mail: jzhao@ust.hk

** This work was financially supported by the Research Grants Council of Hong Kong through GRF 622910.

Towards the study of granular media from the particle scale, the Discrete Element Method has become a particularly popular tool. Starting from the pioneer work by Cundall and Strack[24], the majority of DEM studies have been based on simplified 2D disks or 3D spherical particles with Coulomb's friction law governing the interparticle sliding. While these features may offer advantages in such aspects as contact law formulation and contact detection for DEM, other fundamental properties of real particles may have been inadvertently overlooked. Among many others, particle shape has been considered to be one of the most important properties that affect the granular behavior as a whole. Realistic consideration of real sand particles should take into account such shape factors of particles as *form* (reflected by the degree of particle elongation or flatness), *roundness* (reflective of the degree of sharpness of corners and edges), *sphericity* (reflected by the degree to which the external envelope of the particle approximates that of a true sphere) and *irregularity* (reflected by the number and size of projections and indentations)[25–27]. Frequently, particle interlocking due to irregularity in shape has been observed in sand under shear which may have significant impact on both the kinematic behavior and the strength of a granular system. Accurate characterization and modeling of real particle shape in DEM proves to be a formidable work which may cause numerous theoretical and computational challenges. There have been studies using ellipse/ellipsoid or glued particles for this purpose (See e.g., Ng[28]). These approximations remain far from accurate characterization of the real particle shape and can be computationally expensive in most cases.

It is recognized that an irregular particle shape always causes resistance to the free rolling of particles, and an alternative way of modeling real particle shape might be to consider the rotational resistance among particles instead. In this paper, we shall employ a three dimensional Discrete Element Method to investigate the effect of rotational resistance on the characteristic behavior of granular materials under shear. A rotational resistance model is developed and implemented in the DEM code. The evolution of different sources of anisotropy attributable to the overall strength of granular systems under undrained shear is monitored. The internal structure formed in the granular system, in terms of contact force network, will be closely examined. The force transmission patterns as well as deformation and energy dissipation mechanisms will be identified and analyzed. The bimodal character of force transmission observed by Radjai et al.[20] and others will be examined as well. The unique properties associated with such characteristic states as liquefaction and critical state will be investigated.

II. ROTATIONAL RESISTANCE AND FORMULATION

A three-dimensional Discrete Element Method code has been modified and used for the present study[29]. A linear force-displacement contact law is employed for the study in which the normal stiffness k_n and the tangential stiffness k_t adopt an equal value of $k_n/r = k_t/r = 100\,\text{MPa}$ where r is an averaged radius defined by $r = (r_1 + r_2)/2$, with r_1 and r_2 being the radii of the two particles in contact, respectively. The interparticle sliding is assumed to be governed by Coulomb's friction law wherein a sliding frictional coefficient $\mu = 0.5$ is adopted. In addition, a rotational resistance model is proposed to account for the influence of irregular particle shape.

2.1. Particle Rolling and Rotational Resistance

In most popular DEM codes, such as Itasca PFC3D, spherical particles have been assumed to be freely rotatable, i.e. the particle rolling is a direct consequence of the inter-particle friction and the angular velocity of the particle is updated by the moments calculated from the frictional forces applied to the surface of the particle. Evidently, this approach oversimplifies the particle kinematics and contact behavior, and cannot adequately handle the real case in granular materials mentioned above. We hereby develop a new approach based on spherical particle system. In view of the fact that real granular particles are more often non-spherical and non-rounded than otherwise, the interparticle contact will be frequently in form of plane-to-plane or point-to-plane types. The acute corners of a particle are easily crushed during the deforming process such that point-to-plane contacts are rarely stable enough to sustain large shear. As such, plane-to-plane contact can be regarded as the dominant type of contact. At each of such contacts, the interlocking is considered to be attributable to the resistance to the rolling of contacted particles. In this connection, we introduce a contact moment M_r at the contact plane to restrict the relative rolling between particles. Note that similar measures have been adopted by Ishihara and Oda[30] and Estrada et al.[31]. It is assumed that the extent of this restriction is governed by an

efficient parameter of rolling stiffness which relates M_r with the relative rolling angle between particles according to:

$$M_r = -k_r \theta_r \tag{1}$$

where θ_r is the relative rotation angle between two contacting particles. The rolling stiffness k_r is assumed to be related to the shear stiffness according to $k_r = k_t r^2$[30]. Similar to Coulomb's friction law, we consider a threshold moment

$$M_{\max} = \mu_r f_n l \tag{2}$$

such that $|M_r| \leq M_{\max}$, where μ_r is the rotational resistance coefficient, f_n is the normal force and l is the characteristic length which is related to the particle radii and the penetration depth between particles (See Fig.1). When there is a tendency of relative rolling at a contact, a triangular normal force distribution can be assumed along the contact plane as shown in Fig.1[32,33]. It is normally safe to assume that the penetration depth of the two particles is about 2% of the equivalent radius r. l can then be estimated by $l = w/6 = 2\sqrt{r^2 - (0.99r)^2}/6 \approx 0.05r$. In this way, we may judge whether or not relative rolling will occur at a contact.

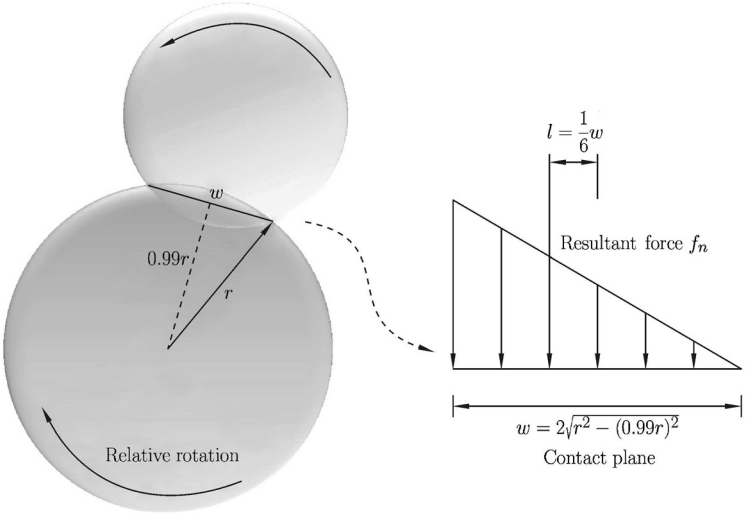

Fig. 1. Contacting particles with a tendency of relative rolling and triangular distribution of normal force.

2.2. Packings with Different Initial States

A total of around 32000 spherical particles with radii ranging from 0.2 mm to 0.6 mm are randomly generated in a cubic box with six rigid frictionless walls. A power law distribution, shown in Fig.2, has been employed to approximate the grain size distribution for a granular medium (in comparison with a log-normal distribution), wherein an exponent $D = 3.63$ is adopted. D has been referred to as the *fractal dimension* by Mair and Hazzard[34]. After a desired number of particles have been generated in the cubic box, we then perform staged isotropic consolidation to generate packings with different initial void ratios. At different stages of consolidation, different frictional coefficients μ are used until the confining pressure reaches the designated value ($p'_0 \approx 190$ kPa here). Table 1 summarizes the various samples prepared for the subsequent shear. e_0 is the initial void ratio of a sample prior to shear.

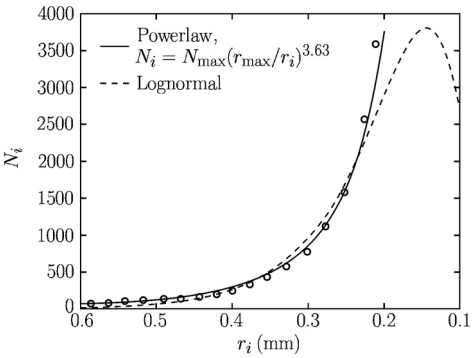

Fig. 2 Size distribution of particles used for packing. N_i is the number of particles with a radius or r_i, and $N_{\max}$ denotes the number of particles with a maximum radius $r_{\max}$ in the packing.

To examine the effect of rotational resistance, triaxial shear tests have been conducted on the various packings prepared above. In particular, we elect to shear the samples under undrained loading

Table 1. **Sample packings to be sheared under undrained condition**

Sample	Initial void ratio e_0	Rotational resistance coefficient μ_r
UR0	0.644	0.0 (no rotational resistance)
UR1	0.647	0.1
UR3	0.648	0.3
UR5	0.649	0.5

conditions. Since only dry particles are involved in the DEM simulation, we approximate the undrained condition in soil mechanics by imposing a constraint of constant volume on the sheared sample (See also Yimsiri and Soga[35]). During the shearing, the horizontal strain is continuously adjusted with the vertical compression to maintain a constant value for the total volume of the assembly. For the different samples shown in Table 1, different rotational resistance coefficients have been used. Note that sample UR0 corresponds indeed to the free rolling case.

2.3. Definitions of Macroscopic Descriptors

We employ the following definition of stress tensor proposed by Christoffersen et al.[36]:

$$\sigma_{ij} = \frac{1}{V}\sum_{c\in N_c} f_i^c d_j^c \tag{3}$$

where V is the total volume of the assembly, N_c is the total number of contacts, $\boldsymbol{f}^c$ is the contact force at a contact and $\boldsymbol{d}^c$ is the branch vector joining the centers of two contacting particles. It is ready from Eq.(3) to derive the mean effective stress and the deviatoric stress $p' = \frac{1}{3}\sigma_{ii}$, $q = \sqrt{\frac{3}{2}\sigma'_{ij}\sigma'_{ij}}$, where σ'_{ij} is the deviatoric part of the stress tensor σ_{ij}. The strain tensor is calculated here according to the displacement gradient at the boundary walls of a sample, i.e., $\varepsilon_{ij} = \partial u_i/\partial x_j$.

It is interesting to explore the shear-induced anisotropy in the study as well. In quantifying anisotropy in a granular assembly, two classes of anisotropy with different mechanisms are distinguished, the *geometrical anisotropy* and the *mechanical anisotropy*[37]. The geometrical anisotropy is defined by the local orientation of contact plane which gives rise to the global anisotropic phenomenon. The mechanical anisotropy, on the other hand, is mainly caused by the external forces and depends heavily on the induced contact forces in relation to the orientation of contact planes. The geometrical anisotropy in an assembly of polydispersive spherical particles can be expressed in terms of the distribution of *contact normals* and *branch vectors*. This paper adopts the following expression of *fabric tensor* proposed by Satake[38] and Oda[39]:

$$\phi_{ij} = \int_{\Theta} E(\Theta)\, n_i n_j \mathrm{d}\Theta \tag{4}$$

where $\boldsymbol{n}$ is the unit vector along the normal direction of the contact plane, Θ characterizes the orientation of $\boldsymbol{n}$ relative to the global coordination system, and $E(\Theta)$ is the distribution probability function. In most cases it suffices to employ the second-order Fourier expansion of $E(\Theta)$ to characterize the contact normals (See e.g., Refs.[40,41]):

$$E(\Theta) = \frac{1}{4\pi}(1 + a_{ij}^c n_i n_j) \tag{5}$$

wherein the second-order anisotropic tensor a_{ij}^c is deviatoric and symmetric, and can be used to characterize the fabric anisotropy. It is easily verified that

$$a_{ij}^c = 15/2\, \phi'_{ij} \tag{6}$$

where ϕ'_{ij} is the deviatoric part of ϕ_{ij}.

Branch vectors may constitute an important part of geometrical anisotropy, especially when the granular assembly comprises of polydispersive or non-spherical particles. The distribution of branch vector may be expressed in a similar way as the contact normals in Eqs.(4) and (5):

$$d_{ij} = \frac{1}{4\pi}\int_{\Theta} \bar{d}(\Theta) n_i n_j \mathrm{d}\Theta \tag{7a}$$

$$\bar{d}(\Theta) = \bar{d}^0(1 + a_{ij}^d n_i n_j) \tag{7b}$$

where

$$a_{ij}^{d} = \frac{15}{2}\frac{d'_{ij}}{\bar{d}^0}$$

is the contribution of branch vector to the geometric anisotropy tensor. It has the same property with a_{ij}^{c}. $\bar{d}^0 = d_{ii}$ is the average branch vector length calculated over different Θ and may differ from $\bar{d}$ which is averaged over all contacts. It is noted that in polydisperse spherical assemblies which will be dealt with in this paper, the branch vectors have normal components only.

The mechanical anisotropy can be split into normal force anisotropy caused by normal contact forces and tangential force anisotropy induced by tangential contact forces, which are, respectively, defined as follows:

$$\chi_{ij}^{n} = \frac{1}{4\pi}\int_{\Theta} \bar{f}^{n}(\Theta) n_i n_j \mathrm{d}\Theta \tag{8a}$$

$$\bar{f}^{n}(\Theta) = \bar{f}^{0}(1 + a_{ij}^{n} n_i n_j) \tag{8b}$$

and

$$\chi_{ij}^{t} = \frac{1}{4\pi}\int_{\Theta} \bar{f}^{t}(\Theta) t_i n_j \mathrm{d}\Theta \tag{9a}$$

$$\bar{f}_i^{t}(\Theta) = \bar{f}^{0}[a_{ik}^{t} n_k - (a_{kl}^{t} n_k n_l) n_i] \tag{9b}$$

where

$$a_{ij}^{n} = \frac{15}{2}\frac{{\chi'^{n}}_{ij}}{\bar{f}^0}, \quad a_{ij}^{t} = \frac{15}{3}\frac{\chi_{ij}'^{t}}{\bar{f}^0}$$

Similar to previous cases, $\bar{f}^0 = \chi_{ii}^{n}$ denotes the average normal force calculated over different Θ and may differ from the average normal force $\bar{f}$ over all contacts. Note that $\bar{f}$ will be used in the sequel to distinguish the strong and weak contact forces.

Collectively, we have now defined a total of four anisotropic tensors, a_{ij}^{c}, a_{ij}^{d}, a_{ij}^{n} and a_{ij}^{t}, which can be conveniently used to characterize the anisotropic behavior originated from distinctive sources in granular material. Since all four tensors are deviatoric in nature, it is handy to use the following deviatoric invariant of each tensor to quantify the degree of anisotropy in each case

$$a_* = \mathrm{sign}(S_r)\sqrt{\frac{3}{2}a_{ij}^{*}a_{ij}^{*}} \tag{10}$$

where the sub/super-script * stands for c, d, n or t corresponding to one of the four cases of anisotropy mentioned above, respectively. S_r is a normalized quantity of the double contraction of a_{ij}^{*} and σ'_{ij} defined below

$$S_r = \frac{a_{ij}^{*}\sigma'_{ij}}{\sqrt{a_{kl}^{*}a_{kl}^{*}}\sqrt{\sigma'_{mn}\sigma'_{mn}}} \tag{11}$$

The prefix $\mathrm{sign}(S_r)$ on the right-hand side of Eq.(10) signifies the relative orientation of the principal direction of a_{ij}^{*} with respect to that of the stress tensor. Consequently, a positive sign of a_{ij}^{*} indicates that the major principal direction of a_{ij}^{*} is closer (e.g., within $\arccos(\sqrt{3}/3)$ for an axisymmetric case) to the major principal direction of the stress tensor, and a negative sign for a_{ij}^{*} if otherwise. Note that a similar definition has been employed by Ouadfel and Rothenburg[40], Gao et al.[42] and Guo and Zhao[43].

III. NUMERICAL RESULTS AND DISCUSSION

3.1. Macro Responses of Different Packings under Undrained Shear

The responses of samples with different rotational resistance coefficients μ_r are shown in Fig.3. As is shown, the four samples demonstrate different responses under undrained shear. UR0 experiences apparent liquefaction after around 7.5% axial strain, while the other three samples all exhibit an obvious phase transformation stage before reaching the critical state. Among them, the response of UR1 is similar to the typical response of a medium dense sand under undrained shear, while the other two share great

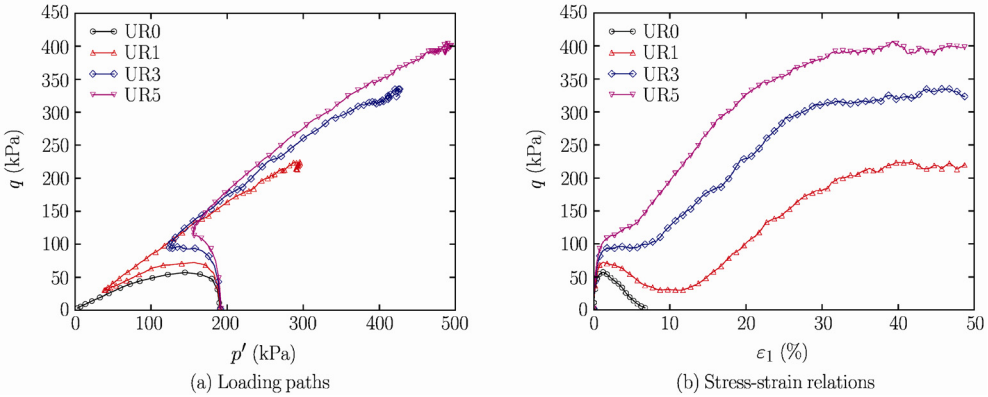

Fig. 3. Undrained macroscopic response of granular assemblies with different rotational resistance coefficients.

resemblance of dense sand responses. The effect of considering rotational resistance is evident from the figure. A sample apparently becomes stronger in consideration of rotational resistance than otherwise. The shear strength of a sample (peak deviatoric stress) increases steadily with the increase of μ_r. In view of this, the three samples, UR1, UR3 and UR5, all possess a looser initial state than UR0 which makes them potentially more prone to liquefaction than UR0 if rotational resistance is not considered. We see that the introduction of rotational resistance may indeed help an otherwise liquefiable sample to develop appreciable resistance to avoid liquefaction. In particular, Sample UR1 experiences a drastic contraction process and a reduction in effective stress up to around 20% of its initial value, but is still able to pull its stress path back at the phase transformation point and develop dilative deformation towards the critical state.

3.2. Stress-force-fabric Relationship

An analytical correlation between the anisotropy and stress, the so-called stress-force-fabric relationship, has been established by Rothenburg[44] and Rothenburg and Bathurst[18] based on DEM study of two-dimensional disk-like particles. The relationship has been further generalized to the three-dimensional case by Chantawarungal[45] with the following form:

$$\sigma_{ij} = \frac{N_c \bar{f} \bar{d}}{3V} \left\{ \delta_{ij} + \frac{2}{5} \left(a^c_{ij} + a^n_{ij} + \frac{3}{2} a^t_{ij} \right) + \frac{2}{35} \left[\left(a^n_{kl} - a^t_{kl} \right) a^c_{kl} \delta_{ij} + \left(4a^n_{il} + 3a^t_{il} \right) a^c_{lj} \right] \right\} \tag{12}$$

where δ_{ij} is the Kronecker delta. In the original equation, Chantawarungal[45] has neglected the contribution by the branch vector. As mentioned before, in assemblies composed of highly polydispersive particles or particles of nonspherical shapes, the contribution from the branch vector could be significant. By including a_d, further manipulation of Eq.(12) readily leads to the following expression of stress-force-fabric relationship in terms of q/p' and the invariants of anisotropic tensors (with the cross products between two anisotropic tensors being neglected):

$$\frac{q}{p'} = \frac{2}{5} \left(a_c + a_d + a_n + \frac{3}{2} a_t \right) \tag{13}$$

For a 2D granular system Voivret et al.[46] have given an expression $q/p' = (a_c + a_d + a_n + a_t)/2$. Note that not all sources of anisotropy contribute positively to the shear strength. For example, consideration of non-spherical particle shape may lead to a negative contribution of a_d to the overall shear strength, as has been noted by Ouadfel and Rothenburg[40].

With the available DEM simulation results, we are able to explore if the correlation is still valid in consideration of rotational resistance. As is shown in Fig.4, the analytical stress-force-fabric relationship in Eq.(13) correlates very well with the DEM simulations, even in the case of UR0. The shear strength of a granular assembly can hence be directly related to its capability of developing anisotropy. It is noticed, however, the employment of rotational resistance does slightly change the critical state stress ratio (or the so-called slope of critical state line). A higher value of μ_r generally leads to a higher stress

ratio at critical state. In essence, different rotational resistance coefficients may lead to different cases of roundness for sand particles, such that they can no longer be treated as the same material. It is hence no surprise that the resultant critical state stress ratio is different. Meanwhile, rotational resistance renders the contacts in the horizontal direction of a sample much harder to be detached and thus tends to facilitate the formation of stronger lateral support. This feature will be discussed later in relation with the bimodal character.

3.2.1. Weight of different anisotropy sources in shear strength

It is also interesting to compare the contributions of different sources of anisotropy to the overall shear strength. Figure 5 presents the relative weights of a_c, a_n, a_t as well as a_d for the four samples. Except for the case of UR0, the normal force anisotropy a_n in general dominates the shear strength by contributing more than 50% in weight to the total value, and is the main bearer that carries the external deviatoric loads. The contact normal anisotropy a_c plays a second important role and contributes around 30%, while the tangential force anisotropy a_t normally contributes less than 20%. The contributing weight of a_d is negligibly small and is only around 2%. Evidently, the mechanical anisotropy (a_n plus a_t) plays a dominant role in resisting the external shear force. The ratios of weights among a_n, a_c and a_t is close to 5:3:2. While consideration of rotational resistance may help increase the shear strength of the material, it does not appear to change the relative weights of the different anisotropies

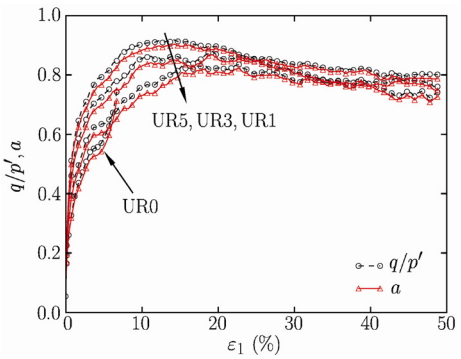

Fig. 4 Correlation of the analytical stress-force-fabric relationship in Eq.(13) (q/p') with DEM simulation for packings considering rotational resistance, $a = 2/5(a_c + a_d + a_n + 3/2a_t)$.

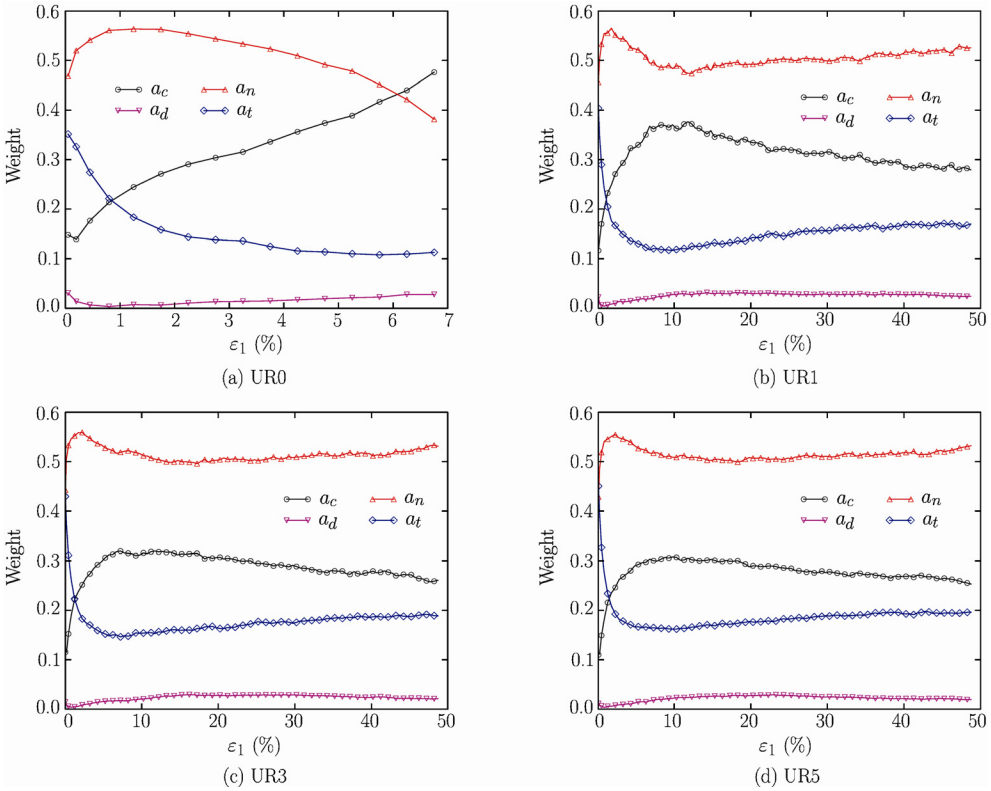

Fig. 5. Contributing weights of various anisotropy sources to the shear strength of samples (including coefficients in Eq.(13) for each term).

in contributing to the overall shear strength.

As for UR0, the weight of a_c is found to increase rapidly and surpasses that of a_n before the sample enters liquefaction. This indicates that at liquefaction, the geometric anisotropy dominates over any mechanical anisotropies in the sample, which appears to be a very special feature associated with liquefaction only. Indeed, from the observation of other samples, the mechanical anisotropy, a_n in particular, has to be dominant in the material strength, in order for a sample to avoid liquefaction.

3.2.2. Characteristics of anisotropy and its evolution

It is interesting to take a quantitative look at the characteristics of anisotropy and its evolution during the loading process. The four anisotropic invariants as defined in Eq.(10) are convenient terms to be monitored. It is noticed that owing to the use of spherical particles with a relatively narrow size distribution, the branch vector anisotropy a_d has been found to contribute less than 3% of the total strength. Its behavior shall not be discussed in detail in this subsection. Since the responses of UR3 and UR5 are quite similar to those of UR1, UR1 has hereby been chosen to demonstrate the characteristics of anisotropy during the undrained shear, in close comparison with the case of UR0. The results are presented in Fig.6. In particular, Radjaï et al.[20] have found that the contact force network within a *dense* granular system under direct shear largely consists of two complementary subnetworks, a weak force subnetwork and a strong force subnetwork. The weak force subnetwork comprises of interparticle contacts with force below the average, while the strong force subnetwork consists of contacts which have greater than average contact forces. The weak force subnetwork has been found largely isotropic and functions to balance the hydrostatic pressure in the assembly. The strong subnetwork is acutely anisotropic and sustains a major proportion of the deviatoric load. It is interesting to examine the validity of this bimodal theory for granular systems with different initial packing states in consideration of rotational resistance. In presenting the results, we have hereby separated the contributions of the weak force subnetwork from the strong force subnetwork, along with the total value, to verify the bimodal character observed by Radjaï et al.[20]. The contribution from the strong force subnetwork is denoted by Γ_{strong}, the part from the weak force subnetwork by Γ_{weak}, and the entire contact network by Γ_{total}.

From the evolution of a_c in UR1 in Fig.6, the rotational resistance appears to enhance the weak contact force subnetwork. a_c in Γ_{weak} has exhibited a surprising positive value from 3.5% to 23% axial strain range. Rotational resistance appears to have reduced the role of the weak force subnetwork as purely a lateral propping system, but contribute more to sharing part of the deviatoric load with the strong force subnetwork. Indeed, in a recent study of the role of weak subnetwork in the buckling of force chains, Tordesillas and Muthuswamy[47] have observed that the introduction of rotational resistance may help to stabilize the force chain structure directly by providing greater rotation resistance which is regarded as a key mechanism of buckling, and it may also facilitate the stabilization of the lateral support from the weak force subnetwork and hence enhance the stability of strong force chains indirectly. We have however noted that at least from a_c of UR1 in Fig.6 the change of role of the weak force subnetwork caused by the rotational resistance is only temporary (e.g., only at certain early deformation stages). When the deformation is large enough (e.g., beyond 30% of axial strain up to the critical state), a_c in Γ_{weak} turns from positive to negative again. The role of weak force subnetwork in UR1 hence returns to its normal way of providing lateral support only, which is consistent with the observation by Radjaï et al.[20].

Different than the cases of a_c, a_n in Γ_{weak} plays a distinctively positive contribution to the overall anisotropy during the entire shear process. This implies that it aligns more in the deviatoric direction rather than perpendicular to it. However, the magnitude of a_n in Γ_{weak} remains small compared to that in Γ_{strong}, and is only 25%∼30% of the latter for UR1. The total a_n is still dominated by the strong force subnetwork. We note that the total a_n is not a simple weighted value of a_n in Γ_{strong} and Γ_{weak}. As such its value is greater than the a_n in either strong or weak subnetwork as shown in Fig.6, unlike the case of a_c. It is noticeable that the contact force anisotropy is mobilized quickly after the application of shear force and develops to its peak value comparable to the steady state value within 5% of axial strain. This is especially apparent in the strong force subnetwork. In contrast, it needs relatively larger deformation for the fabric anisotropy (a_c) to be fully mobilized (greater than 10% axial strain), evidently from the slope of the curves at the initial deformation stage. Not presenting here we have found the difference is clearer in the smaller rotational resistance cases, but not so obvious in the

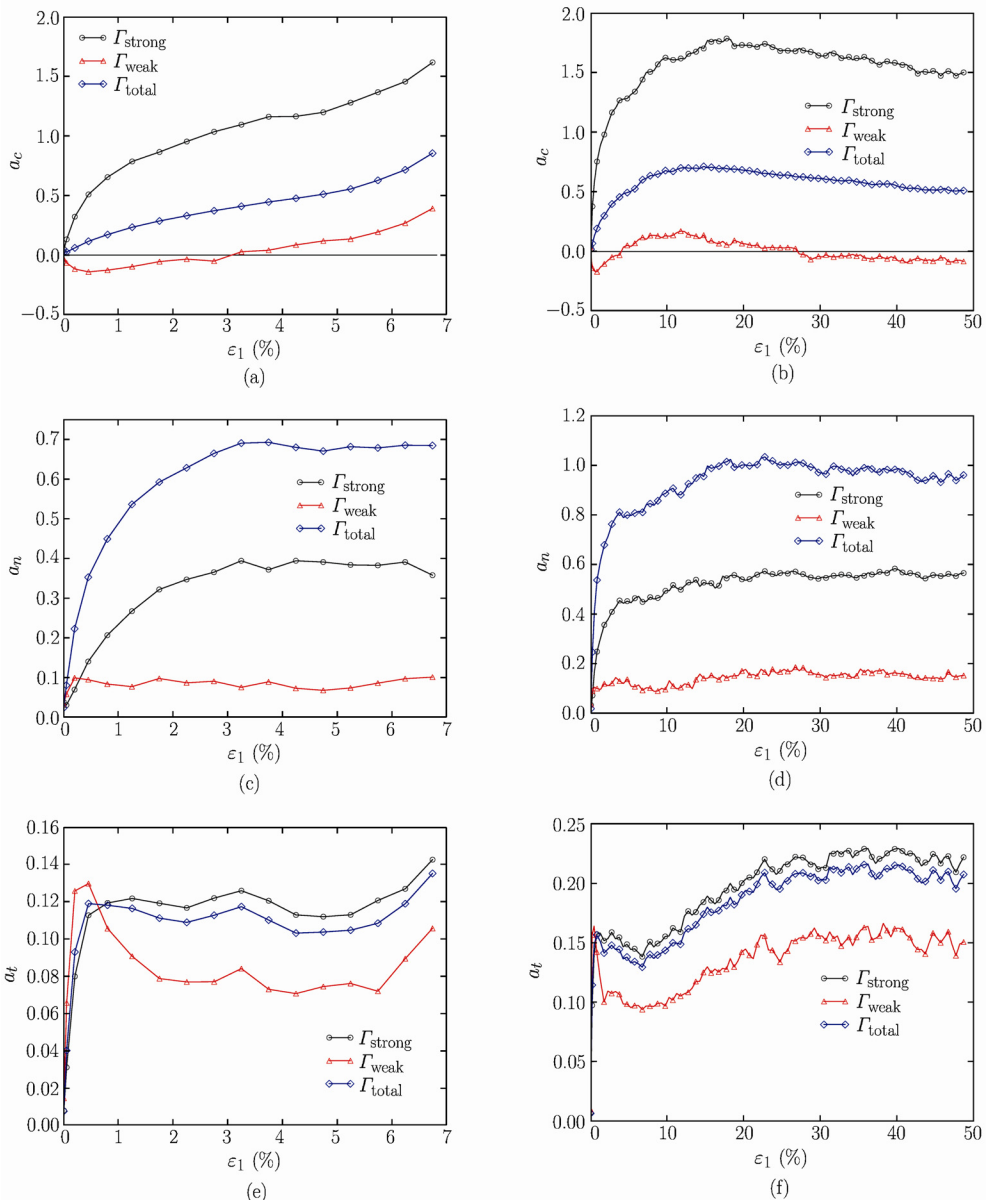

Fig. 6. Evolution of anisotropy in Sample UR0 (a, c, e) and UR1 (b, d, f).

other cases (such as UR5). It is believed that the instantaneous contraction a sample has to experience may attribute to the prolonged process of establishing stable fabric structure and hence steady fabric anisotropy.

Compared to the cases of a_c and a_n, the tangential force anisotropy a_t during the shearing course is much smaller, even in the strong force subnetwork, as is shown in Fig.6. Interestingly, it is observed that upon shearing, a_t can be mobilized instantly (e.g., within 1% axial strain) to a peak, and then drops slightly before regaining its increasing trend as the shearing proceeds. The change is even more drastic than in the a_n case. Meanwhile, the values of a_t in Γ_{strong} and Γ_{total} are found to be close to each other. The contribution from the weak force subnetworks to the total a_t is very small. The evolving curves of a_t are more fluctuated than those for a_n and a_c. The numerous fluctuations in a_t reflect a typical 'slip and stick' mode for frictional contact[48].

In contrast, for UR0, a_c in Γ_{weak} exhibits a quite different behavior. Instead of staying approximately zero, it evolves steadily from negative to positive and finally reaches $a_c = 0.39$ prior to liquefaction.

The total value of a_c in sample UR0 is greater than that in other samples at the same level of axial strain, whereas the values of a_n and a_t observed from Figs.6(c) and 6(e) are much smaller.

3.3. Liquefaction and Critical State

The behavior of granular materials at liquefaction or critical state is particularly interesting, due to their theoretical significance and practical importance. *Liquefaction* has long been regarded as an important attribute to various engineering disasters involving sand. Under undrained or partially drained conditions, rapid shear may generate quick accumulation of excessive pore water pressure which cannot dissipate timely and reduces the effective mean stress sharply. Liquefaction occurs when the effective mean stress in such a process becomes negligibly small and the material can no longer sustain any deviatoric stress according to Coulomb's friction law. *Critical state* refers to a special stage of a granular material at very large strain when continuous flow with constant volume and constant stresses[2] occur. The concept of critical state builds the cornerstone of critical state soil mechanics. Among the four samples that have been treated, UR0 reaches a state of liquefaction, and all the other three samples reach critical state.

It is interesting herein to first compare the internal structure at the two states. A granular system transmits forces through the interparticle contact force network. Many features of the contact force network make it ideal for the study of the characteristics of internal structure. The network reflects not only the interparticle fabric connection but also how the fabric transmits the external load within the granular system. The bimodal character of force transmission suggested by Radjaï et al.[20] has been based on the contact force network. To compare the internal structure formed at the liquefaction state and critical state, we take the cases of UR0 and UR5 as demonstrative examples. Figure 7 presents the final internal structures formed in UR0 and UR5, respectively. Note that in the case of UR0, the thickness of the force chains has been magnified around 20 times to render visibility. Evidently, the critical state reached in UR5 features a clear anisotropic structure with vertical thick column-like strong force chains and very thin weak contact force network which is largely isotropic. This is precisely a clear signature of the bimodal character observed by Radjaï et al.[20]. In contrast, the entire force network at liquefaction in the case of UR0 is very weak, with an average contact force far smaller than that at the critical state in UR5 (over 50 times smaller). The bimodal feature in this network also becomes less distinctive. The entire sample becomes so loose that no sufficiently strong force chains can be established within the system to sustain the small yet existing deviatoric force. In this case, it is observed that even in the weak force subnetwork a certain proportion of contacts have been mobilized to orient more to the vertical direction to share part of the deviatoric force.

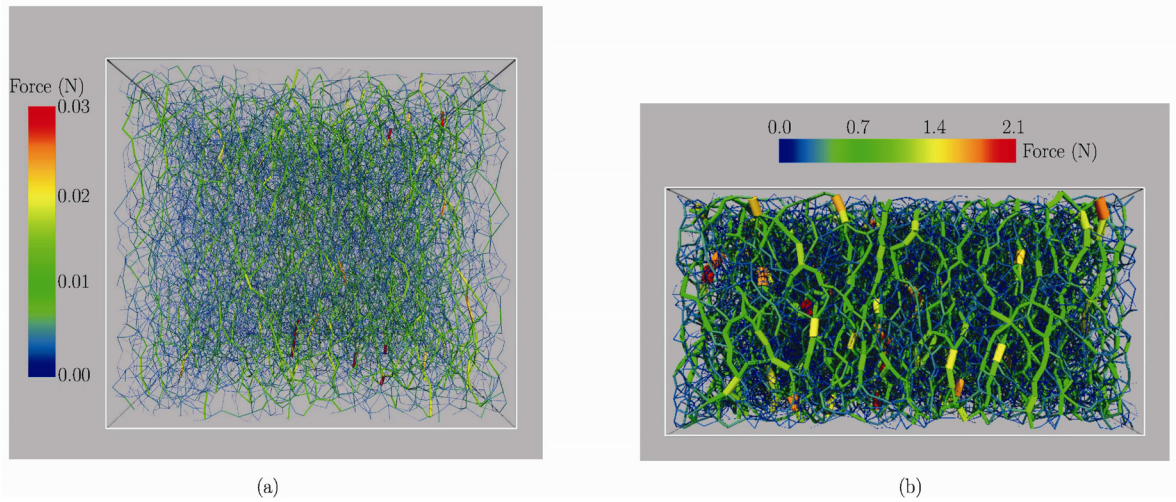

Fig. 7. Force chain network: (a) at the liquefaction state for Sample UR0, and (b) the critical state for Sample UR5.

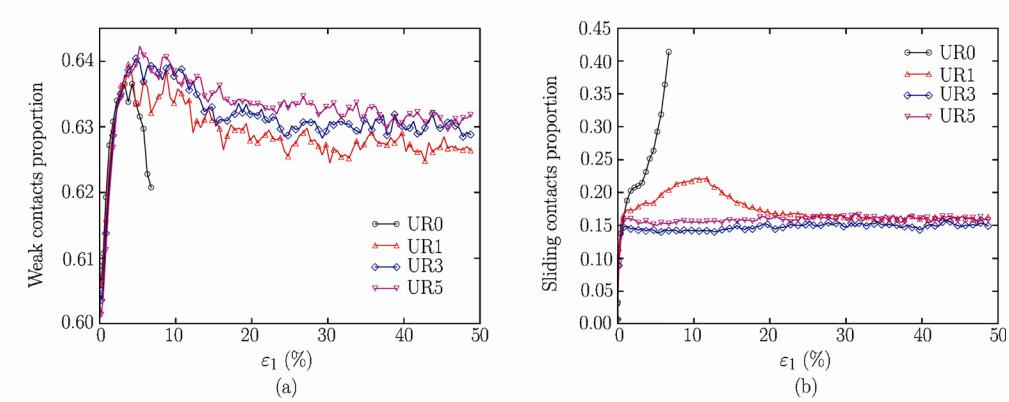

Fig. 8. Proportion of weak force contact (a) and sliding contact (b) in the contact network during the loading course.

It is found that a relatively higher proportion of weak force contacts is present in the force network when rotational resistance is considered. The greater μ_r is, the higher this fraction becomes. The proportions of weak contacts as well as sliding contacts in the contact network for the four cases are depicted in Fig.8. While at the peak stage, all samples have roughly the same proportion of weak contacts. The weak contact weighs a slightly smaller fraction at liquefaction in the case of UR0 than other cases at the critical state. Meanwhile, a granular assembly dissipates energy primarily through interparticle sliding. The proportion of sliding contact can thus be regarded as an indicator of energy dissipation. As shown in Fig.8, at the liquefaction state in UR0, sliding contact accounts for more than 40% of the total contacts in the assembly, in contrast to an approximation of 15% in other cases at critical state. It is also noticed that these sliding contacts are exclusively mobilized in the weak force subnetwork. And the proportion of sliding contacts in weak contacts is around 65% in UR0 at liquefaction, while in other cases this proportion is only about 24% at the critical state. It appears that this fraction of mobilized sliding contacts in weak force contacts may serve as a clearer indicator of the distinction between liquefaction and critical state, as well as the susceptibility to flow liquefaction in granular materials. Note that the percentage of sliding contacts at critical state, along with the critical coordination number, may be affected by interparticle friction (See, e.g., Refs.[21,49]). Other factors in DEM may affect the behavior of critical state. Increase of interparticle friction, for example, has been shown by Thornton[49] to be able to lead to increased critical void ratio but decreases in the percentage of sliding contact and coordination numbers at critical state.

It is also interesting to investigate the effect of rolling resistance on the critical state. Plotted in Fig.9 are the critical state data points and fitting with rotational resistance taken into consideration. To gain a better curve a number of extra tests on samples with different initial void ratios under both

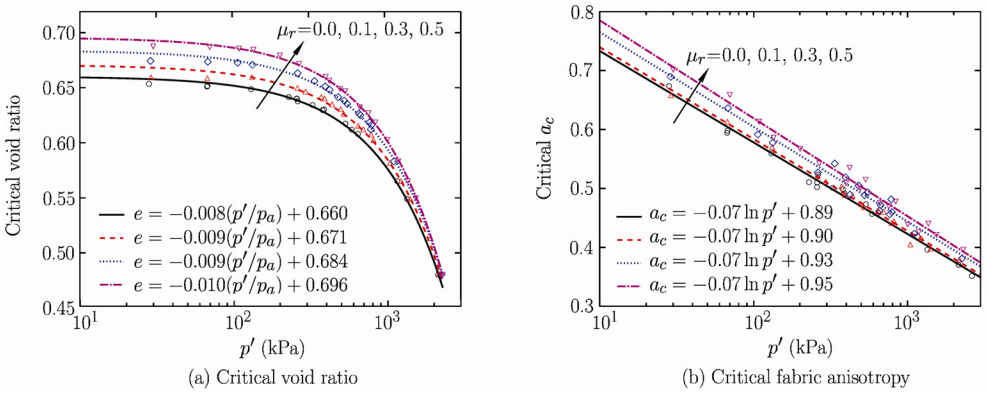

Fig. 9. Critical state lines of samples with different rotational resistance coefficients ($p_a = 1$ atm). Numerical data points are denoted by triangles and diamonds.

drained and undrained shear have been performed for each case of rotational resistance (UR0 has been tested under drained shear to reach critical state for $\mu_r = 0$). A linear relation between critical void ratio e_c and p' has been found for each case of rotational resistance (See also Guo and Zhao[43]. This is consistent with experimental data on Erksak sand[50] and Toyoura sand[51], as well as other numerical results[28]. The different cases of rotational resistance demonstrate roughly parallel critical state lines which possess an identical slope at around -0.009. Higher rotational resistance renders the line higher. Interestingly, a similar linear relation has been found between the critical fabric anisotropy a_c and $\ln p'$, as shown in Fig.9(b). The lines for different cases are parallel to one another at a slope of -0.007 with the greater μ_r case located higher, as in the case of critical void ratio. This is a rather new finding which has not been mentioned in the classic critical state theory. Note that Li and Dafalias[52] have recently proposed a new critical state theory in which the role of fabric anisotropy has been emphasized.

IV. CONCLUSIONS

A micromechanical study on the behavior of granular material under triaxial undrained shear has been presented using a three- dimensional Discrete Element Method with spherical particles. Emphasis is placed on the consideration of rotational resistance as an alternative way to consider the non-spherical particle shape. It has been found that the internal structure formed in a granular body under shear can be characterized by the contact force network. The network is essentially anisotropic and depicts a clear bimodal character as observed by Radjaï et al.[20]. In consideration of rotational resistance, a good correlation between an analytical expression for stress-force-fabric relation and the numerical results on anisotropy has been found still valid, which proves that in granular materials, certain degree of anisotropy has to be developed in order to mobilize adequate shear strength to balance the applied shear. The mechanical anisotropy is found to dominate in the shear strength except in the liquefied sample. In the case of liquefaction, the entire force network becomes very weak, and the bimodal character also becomes less distinctive. The shear strength may be dominated by geometrical anisotropy rather than mechanical anisotropy at liquefaction state. Also, a liquefaction state is always associated with a high proportion of sliding contacts in the weak force contacts. Rotational resistance may help increase the shear strength of the material (see also, Estrada et al.[31]), in particular the liquefaction resistance for a loose sample. It can be seen from the triaxial test results that the critical state can be uniquely characterized by two linear relations between $e - p'$ and $a_c - \ln p'$. Different rotational resistances may shift the critical lines, for both critical void ratio and critical fabric anisotropy, in a translational manner. Greater rotational coefficient generally leads to higher lines for critical e as well as for critical a_c. We note however that the conclusions drawn here may still be subjected to further verification with additional data obtained under more general and complex loading conditions (e.g., rotational shear and/or cyclic loading) and on samples with initial anisotropy. This will be pursued in the future.

References

[1] Been,K. and Jefferies,M., Soil Liquefaction: A Critical State Approach. Taylor & Francis, New York, 2006.

[2] Roscoe,K.H., Schofield,A.N. and Wroth,C.P., On the yielding of soils. *Géotechnique*, 1958, 8(1): 22-53.

[3] Rowe,P.W., The stress-dilatancy relation for static equilibrium of an assembly of particles in contact. *Proceedings of the Royal Society A*, 1962. 269(1339): 500-527.

[4] McDowell,G.R., Bolton,M.D. and Robertson,D., The fractal crushing of granular materials. *Journal of the Mechanics and Physics of Solids*, 1996, 44(12): 2079-2102.

[5] Li,X.S. and Dafalias,Y.F., Dilatancy for cohesionless soils. *Géotechnique*, 2000, 50(4): 449-460.

[6] Gutierrez,M. and Ishihara,K., Non-coaxiality and energy dissipation in granular materials. *Soils and Foundations*, 2000, 40(2): 49-59.

[7] Collins,I.F. and Muhunthan,B., On the relationship between stress-dilatancy, anisotropy, and plastic dissipation for granular materials. *Géotechnique*, 2003, 53(7): 611-618.

[8] Yu,H.S. and Yuan,X., On a class of non-coaxial plasticity models for granular soils. *Proceedings of the Royal Society A*, 2006, 462(2067): 725-748.

[9] Chandler,H.W. and Sands,C.M., The role of a realistic volume constraint in modelling a two dimensional granular assembly. *Journal of the Mechanics and Physics of Solids*, 2007, 55(7): 1341-1356.

[10] Mueth,D.M., Debregeas,G.F., Karczmar,G.S., Eng,P.J., Nagel,S.R. and Jaeger,H.M., Signatures of granular mcirostructure in dense shear flows. *Nature*, 2000, 406: 385-389.

[11] Behringer,R.P., Daniels,K.E., Majmudar,T.S. and Sperl,M., Fluctuations, correlations and transitions in granular materials: statistical mechanics for a non-conventional system. *Philosophical Transactions of the Royal Society A*, 2008, 366(1865): 493-504.
[12] Guo,N. and Zhao,J., Bimodal character of induced anisotropy in granular materials under undrained shear. In: Jiang,M., Liu,F. and Bolton,M. (eds.) Geomechanics and Geotechnics: from Micro to Macro. Taylor & Francis, Shanghai, China, 2011: 513-517.
[13] Zhao,J. and Guo,N., Signature of anisotropy in liquefiable sand under undrained shear. In: Bonelli,S., Dascalu,C. and Nicot,F. (eds.) 9th International Workshop on Bifurcation and Degradation in Geomaterials. Springer, Porquerolles, France, 2011: 45-51.
[14] Zhao,J. and Guo,N., Unique critical state characteristics in granular media considering fabric anisotropy. *Géotechnique*, 2013, 63(8): 695-704.
[15] Ishihara,K., Liquefaction and flow failure during earthquakes. *Géotechnique,* 1993, 43(3): 351-415.
[16] Li,X.S. and Dafalias,Y.F., Anisotropic critical state theory: role of fabric. *Journal of Engineering Mechanics*, 2012, 138(3): 263-275.
[17] Zhao,J. and Guo,N., A new definition on critical state of granular media accounting for fabric anisotropy. In: Powders and Grains 2013: AIP Conference Proceedings, 2013, 1542: 229-232.
[18] Zhao,J., Guo,N. and Li,X.S., Unique quantification of critical state in granular media considering fabric anisotropy. In Yang,Q., Zhang,J.M., Zheng,H. and Yao,Y.P. (eds.) Constitutive Modeling of Geomaterials: Advances and New Application, Proceedings of the Second International Symposium on Constitutive Modeling of Geomaterials. Springer, Beijing, China, 2013: 247-252.
[19] Radjaï,F., Troadec,H. and Roux,S., Key features of granular plasticity. In: Antony,S.J., Hoyle,W. and Ding,Y. (eds.) Granular Materials: Fundamentals and Applications. The Royal Society of Chemistry. Cambridge, UK, 2004.
[20] Rothenburg,L. and Bathurst,R.J., Analytical study of induced anisotropy in idealized granular materials. *Géotechnique*, 1989, 39(4): 601-614.
[21] Chang,C.S., Chao,S.J. and Chang,Y., Estimates of elastic moduli for granular material with anisotropic random packing structure. *International Journal of Solids and Structures*, 1995, 32(14): 1989-2008.
[22] Radjaï,F., Wolf,D.E., Jean,M. and Moreau,J.J., Bimodal character of stress transmission in granular packings. *Physical Review Letters*, 1998, 80(1): 61-64.
[23] Rothenburg,L. and Kruyt,N.P., Critical state and evolution of coordination number in simulated granular materials. *International Journal of Solids and Structures*, 2004, 41(21): 5763-5774.
[24] Kruyt,N.P. and Antony,S.J., Force, relative-displacement, and work networks in granular materials subjected to quasistatic deformation. *Physical Review E*, 2007, 75(5): 051308.
[25] Antony,S.J. and Kruyt,N.P., Role of interparticle friction and particle-scale elasticity in the shear-strength mechanism of three-dimensional granular media. *Physical Review E*, 2009, 79(3): 031308.
[26] Cundall,P.A. and Strack,O.D.L., A discrete numerical model for granular assemblies. *Géotechnique,* 1979, 29(1): 47-65.
[27] Blott,S.J. and Pye,K., Particle shape: a review and new methods of characterization and classification. *Sedimentology*, 2008, 55(1): 31-63.
[28] Mollon,G. and Zhao,J., Fourier-Voronoi-based generation of realistic samples for discrete modeling of granular materials. *Granular Matter*, 2012, 14(5): 621-638.
[29] Mollon,G. and Zhao,J., Generating realistic 3D sand particles using Fourier descriptors. *Granular Matter*, 2013, 15(1): 95-108.
[30] Ng,T.-T., Discrete element method simulations of the critical state of a granular material. *International Journal of Geomechanics*, 2009, 9(5): 209-216.
[31] Abe,S., Place,D. and Mora,P., A parallel implementation of the lattice solid model for the simulation of rock mechanics and earthquake dynamics. *Pure and Applied Geophysics*, 2004, 161(11-12): 2265-2277.
[32] Ishihara,K. and Oda,M., Rolling resistance at contacts in simulation of shear band development by DEM. *Journal of Engineering Mechanics*, 1998, 124(3): 285-292.
[33] Estrada,N., Taboada,A. and Radjaï,F., Shear strength and force transmission in granular media with rolling resistance. *Physical Review E*, 2008, 78(2): 021301.
[34] Jiang,M.J., Yu,H.-S. and Harris,D., A novel discrete model for granular material incorporating rolling resistance. *Computers and Geotechnics*, 2005, 32(5): 340-357.
[35] Jiang,M.J., Yu,H.-S. and Harris,D., Bond rolling resistance and its effect on yielding of bonded granulates by DEM analyses. *International Journal for Numerical and Analytical Methods in Geomechanics*, 2006, 30(8): 723-761.
[36] Mair,K. and Hazzard,J.F., Nature of stress accommodation in sheared granular material: Insights from 3D numerical modeling. *Earth and Planetary Science Letters*, 2007, 259(3-4): 469-485.

[37] Yimsiri,S. and Soga,K., DEM analysis of soil fabric effects on behaviour of sand. *Géotechnique*, 2010, 60(6): 483-495.
[38] Christoffersen,J., Mehrabadi,M.M. and Nemat-Nasser,S., A micromechanical description of granular material behavior. *Journal of Applied Mechanics*, 1981, 48(2): 339-344.
[39] Cambou,B., Dubujet,P. and Nouguier-Lehon,C., Anisotropy in granular materials at different scales. *Mechanics of Materials*, 2004, 36(12): 1185-1194.
[40] Satake,M., The role of the characteristic line in static soil behavior. In: IUTAM symposium on Deformation and Failure of Granular Materials. A. A. Balkema, Delft, 1982: 63-68.
[41] Oda,M., Fabric tensor for discontinuous geological materials. *Soils and Foundations*, 1982, 22(4): 96-108.
[42] Ouadfel,H. and Rothenburg,L., 'Stress-force-fabric' relationship for assemblies of ellipsoids. *Mechanics of Materials*, 2001, 33(4): 201-221.
[43] Sitharam,T.G., Vinod,J.S. and Ravishankar,B.V., Post-liquefaction undrained monotonic behaviour of sands: experiments and DEM simulations. *Géotechnique,* 2009, 59(9): 739-749.
[44] Gao,Z., Zhao,J. and Yao,Y., A generalized anisotropic failure criterion for geomaterials. *International Journal of Solids and Structures*, 2010, 47(22-23): 3166-3185.
[45] Guo,N. and Zhao,J., The signature of shear-induced anisotropy in granular media. *Computers and Geotechnics*, 2013, 47: 1-15.
[46] Rothenburg,L., Micromechanics of Idealized Granular Systems. Ph.D. thesis, Carleton University, 1980.
[47] Chantawarungal,K., Numerical Simulations of Three Dimensional Granular Assemblies. Ph.D. thesis, University of Waterloo, 1993.
[48] Voivret,C., Radjaï,F., Delenne,J.Y. and El Youssoufi,M.S., Multiscale force networks in highly polydisperse granular media. *Physical Review Letters*, 2009, 102(17): 178001.
[49] Tordesillas,A. and Muthuswamy,M., On the modeling of confined buckling of force chains. *Journal of the Mechanics and Physics of Solids,* 2009, 57(4): 706-727.
[50] Johnson,K., Contact Mechanics. Cambridge University Press, London, 1985.
[51] Thornton,C., Numerical simulations of deviatoric shear deformation of granular media. *Géotechnique,* 2000, 50(1): 43-53.
[52] Been,K., Jefferies,M.G. and Hachey,J., The critical state of sands. *Géotechnique*, 1991, 41(3): 365-381.